

# Multiscale Texture Extraction with Hierarchical $(BV, G_p, L^2)$ Decomposition

Liming Tang · Chuanjiang He

Published online: 7 June 2012  
© Springer Science+Business Media, LLC 2012

**Abstract** In this paper, we first present a hierarchical  $(BV, G_p, L^2)$  variational decomposition model and then use it to achieve multiscale texture extraction which offers a hierarchical, separated representation of image texture in different scales. The starting point is the use of the variational  $(BV, G_p, L^2)$  decomposition; a given image  $f \in L^2(\Omega)$  is decomposed into a sum of  $u_0 + v_0 + r_0$ , where  $(u_0, v_0) \in (BV(\Omega), G_p(\Omega))$  is the minimizer of an energy functional  $E(f, \lambda_0; u, v)$  and  $r_0$  is the residual (i.e.  $r_0 = f - u_0 - v_0$ ). In this decomposition,  $v_0$  represents the fixed scale texture of  $f$ , which is measured by the parameter  $\lambda_0$ . To achieve a multiscale representation, we proceed to capture essential textures of  $f$  which have been absorbed by the residuals. Such a goal can be achieved by iterating a refinement decomposition to the residual of the previous step, i.e.  $r_i = u_{i+1} + v_{i+1} + r_{i+1}$ , where  $(u_{i+1}, v_{i+1})$  is the minimizer of  $E(r_i, \lambda_0/2^{i+1}; u, v)$ . In this manner, we can obtain a hierarchical representation of  $f$ . In addition, we discuss some theoretical properties of the hierarchical  $(BV, G_p, L^2)$  decomposition and give its numerical implementation. Finally, we apply this hierarchical decomposition to the multiscale texture extraction. The performance of this method is demonstrated with both synthetic and real images.

**Keywords** Multiscale texture extraction · Variational decomposition · Hierarchical decomposition · Duality · Projection algorithm · Fixed point iteration scheme

## 1 Introduction

Texture is an important element in the computer vision and has been analyzed by many researchers. A wide variety of textures are carried out by a multitude of important applications such as remote sensing, medical diagnosis, document analysis, target detection, and so on, still the analysis of textured images is widely recognized as a difficult and challenging problem which is demonstrated by the number of different texture definitions attempted by vision researchers [37, 40].

Texture is always a primary visual cue for pattern recognition and relates to the visual perception of coarseness or smoothness of image features. When it is defined in a quantitative sense, texture is a property that relates to the nature of the variability of pixel values. A visually smoother texture would contain only slight changes in digital number (DN) values over an area while a visually coarse texture would contain many abrupt changes in DN values over an area [17]. The texture model involves basic gray-level (or color) texture primitives that form texture elements, called *textons* [26] or *texels* [21], built from one or several primitives. Several researchers have classified textures into two large groups [37]: *microtextures* (primitives or texture elements) and *macrotextures* (the hierarchy of spatial arrangements of those primitives).

In general, texture analysis includes the following three major issues [32, 37]. The first is texture discrimination based on image partitioning corresponding to different textures, the second is texture classification which categorizes the texture into a finite number of defined classes, and the last is shape extraction from texture, usually reconstruction of 3D-surface geometry from texture information. Of all these areas of texture analysis, texture extraction may be the most important preliminary work. Texture extraction is to

---

L. Tang · C. He (✉)  
College of Mathematics and Statistics, Chongqing University,  
Chongqing 401331, P.R. China  
e-mail: [cjhe@cqu.edu.cn](mailto:cjhe@cqu.edu.cn)

detect the texture primitives or elements from textured image by some image processing techniques. It is the foundation of successful texture analysis and processing, for the extracted textures directly affect the quality of the follow-up processes.

Due to the importance of texture extraction in the area of texture analysis, many different texture extracting methods have been developed, which can be categorized into four major classes [29, 37], characterized as the statistical, structural, model-based and frequency-based. Statistical approaches are based on gray-level distribution of texture element. The simplest method is to describe texture by using the moment of gray-level histogram which can be demonstrated as a texture measure. However, this method does not take into account the spatial information of pixels. Some improved works has been done by calculating the variety of different pixel relationships. By far the most prevalent technique used for deriving texture measures is the use of the gray-level co-occurrence matrix (GLCM) [21, 22]. This technique uses a spatial co-occurrence matrix that computes the relationships of pixel values and then uses these values to compute some statistical properties from these matrices, such as contrast, energy, entropy and correlation coefficient etc.

Structural approaches are based on the theory that textures are composed of regular and repeating elements called primitives, and then texture extraction is identified as a process of determining these primitives and quantitatively analyzing the rules of their arrangement. For example, Hay and Niemann presented a structural method for analyzing texture from forested scenes [23]. Tuceryan and Jain used the Voronoi tessellation features to texture analysis [50]. But structural method is limited because it requires large amounts of information to characterize texture adequately.

Model-based approaches attempt to find stochastic processes that are able to model texture, such as Markov random fields [11, 20], fractal features [16, 39, 44], autoregressive model [1] and multi-resolution simultaneous autoregressive model [31]. These techniques have a common feature that they can describe texture by using small amounts of parameters and have succeed in analyzing microtextures, but they are not very useful for macrotextures situations where little is known about the texture, or more than one texture exists.

Frequency-based approach is called signal processing method, which relies on the information derived from local operators and statistical attributes of images in the frequency domain, such as Fourier power spectrum method [2], Gabor filters [9, 18, 25], Pyramid wavelet transform [30, 35], Tree wavelet transform [33, 35], Wigner distribution [24, 42] and discrete cosine transform (DCT) [3].

It has been argued that a human visualizes a scene in multiple scales [19, 28, 41]. Then multiscale approaches

are appropriate for texture extraction because a single scale may be not a perfect simulation of the human visual perception (HVP) to texture elements. In order to achieve reliable texture information in different scales, both the large-scale and small-scale behaviors should be investigated and incorporated appropriately. Thus, a natural way to address this problem is the multiscale analysis. Frequency-based methods, trying to characterize texture through filter responses directly, such as Gabor filter [9, 18, 25] and wavelet transform [30, 33, 35] can produce a good multiscale texture extraction. These two multiscale techniques transforming images into a hierarchical representation can achieve a good simulation of the HVP.

Recently, an image decomposition method based on variational theory has received more and more attention and has been studied by many researchers (e.g., [4, 6–8, 10, 14, 15, 27, 34, 38, 46–49]). It can achieve the decomposition of a given image by minimizing an energy functional and may be quite effective for texture extraction, since the given image  $f$  is decomposed in to  $u + v$  or  $u + v + r$ , in which  $v$  exactly represents texture component of  $f$ . However, more of the known variational decomposition models can only be used as the fixed scale texture extraction, since they adopt the fixed scale parameter to measure texture. Tadmor et al. have proposed the hierarchical  $(BV, L^2)$  decomposition [48, 49] and hierarchical  $(BV, L^1)$  decomposition [8, 47], but they are not the best for the multiscale texture extraction because neither  $L^2(\Omega)$  nor  $L^1(\Omega)$  is suitable function space to model oscillatory patterns [34].

In this paper, we focus on multiscale texture extraction based on variational image decomposition. To accomplish this, we first propose a hierarchical  $(BV, G_p, L^2)$  variational decomposition model, and then we use it to achieve a multiscale texture extraction. We here adopt  $(BV, G_p, L^2)$  decomposition because  $G_p(\Omega)$  is a very suitable function space to model oscillatory patterns [51, 52]; in addition, the  $G_p$ -norm is easier to solve in practice. Unlike the original fixed scale  $(BV, G_p, L^2)$  variational decomposition, in our hierarchical decomposition, the scale parameter used to measure the texture is not a fixed threshold, but varies over a sequence of bipartite scales. So, this hierarchical decomposition enables us to successively capture the oscillation of  $f$  which lies in the intermediate scale spaces between  $L^2(\Omega)$  and  $G_p(\Omega)$ . Then, the extracted texture of  $f$  is not predetermined but resolved in terms of layers of intermediate scales.

The rest of this paper is organized as follows. Section 2 introduces some backgrounds that are much related to the present paper. Section 3 presents the hierarchical  $(BV, G_p, L^2)$  decomposition. Section 4 shows some properties of this hierarchical decomposition. The numerical implementation for the hierarchical decomposition is given in Sect. 5. In Sect. 6, we apply the hierarchical decomposition to achieve a multiscale texture extraction. This paper is summarized in Sect. 7.

## 2 Backgrounds

### 2.1 Some Function Spaces and Known Results

The use of different function spaces is a common tool in image processing, especially in image decomposition. Here we recall the definition of some function spaces which are much relative to our present work.

**Definition 1** Let  $\Omega \subset \mathbb{R}^2$  be an open subset with Lipschitz boundary, then  $BV(\Omega)$  is a subspace of  $L^1(\Omega)$  such that the following quantity, called the  $BV$ -seminorm or total variation (TV), is finite.

$$|u|_{BV(\Omega)} = \sup \left\{ \int_{\Omega} u \operatorname{div}(\vec{\varphi}) dx \mid \vec{\varphi} \in C_c^1(\Omega, \mathbb{R}^2), \|\vec{\varphi}\|_{L^\infty(\Omega)} \leq 1 \right\}.$$

Further,  $\|u\|_{BV(\Omega)} = \|u\|_{L^1(\Omega)} + |u|_{BV(\Omega)}$  is called the  $BV$ -norm.

The function space  $BV(\Omega)$  plays a key role in the Rudin-Osher-Fatemi (ROF) model [43] (i.e.,  $(BV, L^2)$  decomposition). Meyer [34] has investigated this model and dissatisfied with the results, then he introduced a space  $G(\Omega)$  to model oscillatory patterns. This space happens to be very close to the dual space of  $BV(\Omega)$ . In such a space, oscillatory functions have a small norm, which is a useful property to capture the texture in the energy minimization process. Here we recall the definition of  $G(\Omega)$ .

**Definition 2**  $G(\Omega)$  consists of all the distributions which can be written as

$$v = \partial_x g_1 + \partial_y g_2 = \operatorname{div}(\vec{g}), \quad \vec{g} \in L^\infty(\Omega, \mathbb{R}^2).$$

$G(\Omega)$  can be endowed with the norm

$$\|v\|_{G(\Omega)} = \inf \{ \|\vec{g}\|_{L^\infty(\Omega)} \mid v = \operatorname{div}(\vec{g}), \vec{g} \in L^\infty(\Omega, \mathbb{R}^2) \},$$

here,  $\|\vec{g}\|_{L^\infty(\Omega)} = \operatorname{ess\,sup} \sqrt{g_1^2 + g_2^2}$ .

The main properties of  $G(\Omega)$  are given below.

**Lemma 1** [34] Let  $u \in W_0^{1,1}(\Omega) \subset BV(\Omega)$  and  $v \in G(\Omega)$ . Then

$$\int_{\Omega} uv dx \leq \|v\|_{G(\Omega)} \int_{\Omega} |\nabla u| dx,$$

where  $\nabla u$  is the weak derivation of  $u$ . As a consequence of this lemma we have the following corollary.

**Corollary 1** For any  $u \in W_0^{1,1}(\Omega) \subset BV(\Omega)$  and  $v \in G(\Omega)$ , we have

$$\int_{\Omega} |\nabla u| dx = \sup \left\{ \int_{\Omega} uv dx; v \in G(\Omega), \|v\|_{G(\Omega)} \leq 1 \right\},$$

$$\|v\|_{G(\Omega)} = \sup \left\{ \int_{\Omega} uv dx; u \in W_0^{1,1}(\Omega), \int_{\Omega} |\nabla u| dx \leq 1 \right\}.$$

From this corollary, we can obtain that  $G(\Omega)$  is actually the dual space  $W^{-1,\infty}(\Omega)$  (equipped with dual space) of the normed space  $W_0^{1,1}(\Omega)$  equipped with norm  $\|u\|_{W_0^{1,1}} = \int_{\Omega} |\nabla u| dx$ , which is identical with the result in [27]. The next result of this corollary explains why the function space  $G(\Omega)$  is a very good one to model oscillatory patterns.

Due to the nature of  $G$ -norm, it is quite difficult to compute in practice. To address this problem,  $G(\Omega)$  is replaced by another larger function space  $G_p(\Omega)$  with  $1 \leq p < \infty$  for oscillatory patterns in [51, 52].  $G_p(\Omega)$  is defined as the following.

**Definition 3**  $G_p(\Omega)$  consists of all the distributions which can be written as

$$v = \partial_x g_1 + \partial_y g_2 = \operatorname{div}(\vec{g}), \quad \vec{g} \in L^p(\Omega, \mathbb{R}^2).$$

$G_p(\Omega)$  can be endowed with the norm

$$\|v\|_{G_p(\Omega)} = \inf \{ \|\vec{g}\|_{L^p(\Omega)} \mid v = \operatorname{div}(\vec{g}), \vec{g} \in L^p(\Omega, \mathbb{R}^2) \}.$$

The oscillatory functions have small  $G_p$ -norm too, and such a norm may be easier to compute than the  $G$ -norm in practice. Moreover, if  $p \rightarrow \infty$ ,  $G_p(\Omega)$  approximate  $G(\Omega)$ . Similarly, the function space  $G_p(\Omega)$  is exactly the dual space  $W^{-1,p}(\Omega)$  of the normed space  $W_0^{1,q}(\Omega)$  equipped with norm  $\|u\|_{W_0^{1,q}} = (\int_{\Omega} |\nabla u|^q dx)^{1/q}$  with  $1/p + 1/q = 1$ .

*Remark 1* Since  $G(\Omega)$  is exactly the dual space  $W^{-1,\infty}(\Omega)$  of  $W_0^{1,1}(\Omega)$ , and  $G_p(\Omega)$  is the dual space  $W^{-1,p}(\Omega)$  ( $1 \leq p < \infty$ ) of  $W_0^{1,q}(\Omega)$ , by the Sobolev imbedding theorems, we have  $\|v\|_{G_p(\Omega)} \leq C_{\Omega} \|v\|_{G(\Omega)}$  where  $C_{\Omega}$  is a constant which is independent of  $v$  but  $\Omega$ .

*Example* Let  $m > 0, x \in \Omega = [0, \pi/2], v(x) = \cos(mx)$  and  $g(x) = \frac{1}{m} \sin(mx) + c$ , then  $v = g'$ . We have the following:

- (1)  $\|v\|_{G(\Omega)} = \frac{1}{m}$ . Note that  $\|v\|_{G(\Omega)} \rightarrow 0$  as  $m \rightarrow \infty$ .
- (2) Without loss of generality, assume  $m > 1$ , we have

$$\begin{aligned} \|v\|_{G_p(\Omega)} &= \left( \int_0^{\frac{\pi}{2}} |g(x)|^p dx \right)^{1/p} \\ &= \left( \frac{1}{m^p} \int_0^{\frac{\pi}{2}} |\sin(mx)|^p dx \right)^{1/p} \\ &= \left( \frac{1}{m^{p+1}} \int_0^{\frac{m\pi}{2}} |\sin t|^p dt \right)^{1/p} \leq \left( \frac{\pi}{2} \right)^{1/p} \frac{1}{m}. \end{aligned}$$

And note that  $\|v\|_{G_p(\Omega)} \rightarrow 0$  as  $m \rightarrow \infty$ .

This simple example shows that an oscillatory function has small  $G$ -norm as well as small  $G_p$ -norm, both which approach to zero as the frequency of oscillations increases. In addition, the  $G_p$ -norm is weaker than the  $G$ -norm. So using  $G_p$ -norm to measure oscillatory function, we also can exactly capture the texture during the energy minimization process.

### 2.2 The $(BV, G_p, L^2)$ Decomposition

A grayscale image can be represented by a  $L^2$ -function,  $f : (x, y) \in \Omega \rightarrow \mathbb{R}$ , where  $\Omega$  is an open, bounded and connected subset of  $\mathbb{R}^2$ , typically a rectangle or a square [5, 13, 45]. We focus on the decomposition of  $f$  into three components, i.e.  $f = u + v + r$  where  $u$  represents piecewise smooth (cartoon or structure) component of  $f$ ,  $v$  represents the oscillatory component of  $f$ , which is just what we need (i.e. texture), and  $r$  represents residual. Here are two classical examples of image decomposition by variational approaches which are rather related to our present work.

A celebrated variational decomposition is the  $(BV, G)$  decomposition model proposed by Meyer in [34], which is achieved by solving the following variational problem:

$$\inf_{u,v} \{ |u|_{BV(\Omega)} + \lambda \|v\|_{G(\Omega)}, f = u + v \}. \tag{1}$$

The  $(BV, G)$  decomposition is a better model to extract texture in theory, because it uses a suitable function space  $G(\Omega)$  to describe the oscillatory function, i.e., the oscillatory functions have small  $G$ -norm. However, it cannot be directly solved in practice due to the nature of the  $G$ -norm [4, 6, 7, 51, 52], there is no standard calculation of the associated Euler-Lagrange equation for (1).

Vese and Osher [51, 52] were the first to overcome this difficulty by replacing the space  $G(\Omega)$  with  $G_p(\Omega)$  ( $1 \leq p < \infty$ ). And then the  $(BV, G)$  decomposition model (1) is approximated by the following minimization problem:

$$\inf_{u,v} \{ E(f, \lambda; u, v) = |u|_{BV(\Omega)} + \mu \|f - u - v\|_{L^2(\Omega)}^2 + \lambda \|v\|_{G_p(\Omega)} \}, \tag{2}$$

where  $\mu, \lambda > 0$  are tuning parameter; in addition, parameter  $\lambda$  can be seen as a scale factor to measure the extracted texture. The first term of  $E(f, \lambda; u, v)$  insures that  $u \in BV(\Omega)$ , the second term gives us  $f \approx u + v$ , while the third term is a penalty on the norm in  $G_p(\Omega)$  of  $v$ . By solving (2), we obtain a decomposition of  $f$ ,  $f = u + v + r$  such that  $u \in BV(\Omega)$ ,  $v \in G_p(\Omega)$  and  $r \in L^2(\Omega)$ . We here call it  $(BV, G_p, L^2)$  decomposition.

Then we would like to list some other related works on numerically solving  $(BV, G)$  decomposition. Osher, Solé, and Vese [38] proposed a simplified approximated method

by replacing  $G(\Omega)$  with  $H^{-1}(\Omega)$ , the dual space of  $H_0^1(\Omega)$ . Le and Vese [27] introduced the Dirac function in (2) to compute the  $G_1$ -norm of  $v$ . Aujol, Aubert, Blanc-Féraud and Chambolle [6, 7] defined a convex closed subset of  $G(\Omega)$  and then the oscillation component was modeled as the orthogonal projection on this subset. Weiss, Aubert and Blanc-Féraud [53] proposed an efficient algorithm based on Nesterov scheme [36] for TV minimization, which was used to solve  $(BV, G)$  model.

In what follows, to simplify the notations, we always write  $BV, G_p$  and  $L^2$  instead of  $BV(\Omega), G_p(\Omega)$  and  $L^2(\Omega)$ , respectively.

### 3 Hierarchical $(BV, G_p, L^2)$ Decomposition

In the original  $(BV, G_p, L^2)$  decomposition model (2), the parameter  $\lambda$  can be seen as a scale factor used to measure the extracted texture. If the value of  $\lambda$  is initially chosen to be very large such that, then only the smaller scale texture (coarser texture) can be extracted, and the larger scale texture (smoother texture) is swept into residual component. If  $\lambda$  is too small, however, all the textures are extracted indiscriminately, regardless of their distinct scales. Figure 1 shows the comparison of the decomposition results of model (2) taking different values of  $\lambda$ .

In our present study, to achieve a multiscale texture extraction, we propose a hierarchical  $(BV, G_p, L^2)$  decomposition which simulates hierarchical  $(BV, L^2)$  decomposition proposed by Tadmor, Nezzar and Vese [48]. The scale parameter  $\lambda$  in (2) is not a fixed threshold but varies over a sequence. We start with a larger value of the initial scale parameter  $\lambda$ , and then gradually capture the missing larger scale texture by decreasing the value of  $\lambda$ . The detail is as follows.

For a given scale  $\lambda$ , the minimizer of  $E(f, \lambda; u, v)$  is interpreted as a decomposition,  $f = u_\lambda + v_\lambda + r_\lambda$ , such that  $v_\lambda$  captures textures in the scale  $1/\lambda$ , while the textures above  $1/\lambda$  remain unresolved in  $r_\lambda$ , i.e.,  $r_\lambda$  consists of significant textures when viewed under a larger scale than  $1/\lambda$ , say  $2/\lambda$ :

$$r_\lambda = u_{\lambda/2} + v_{\lambda/2} + r_{\lambda/2},$$

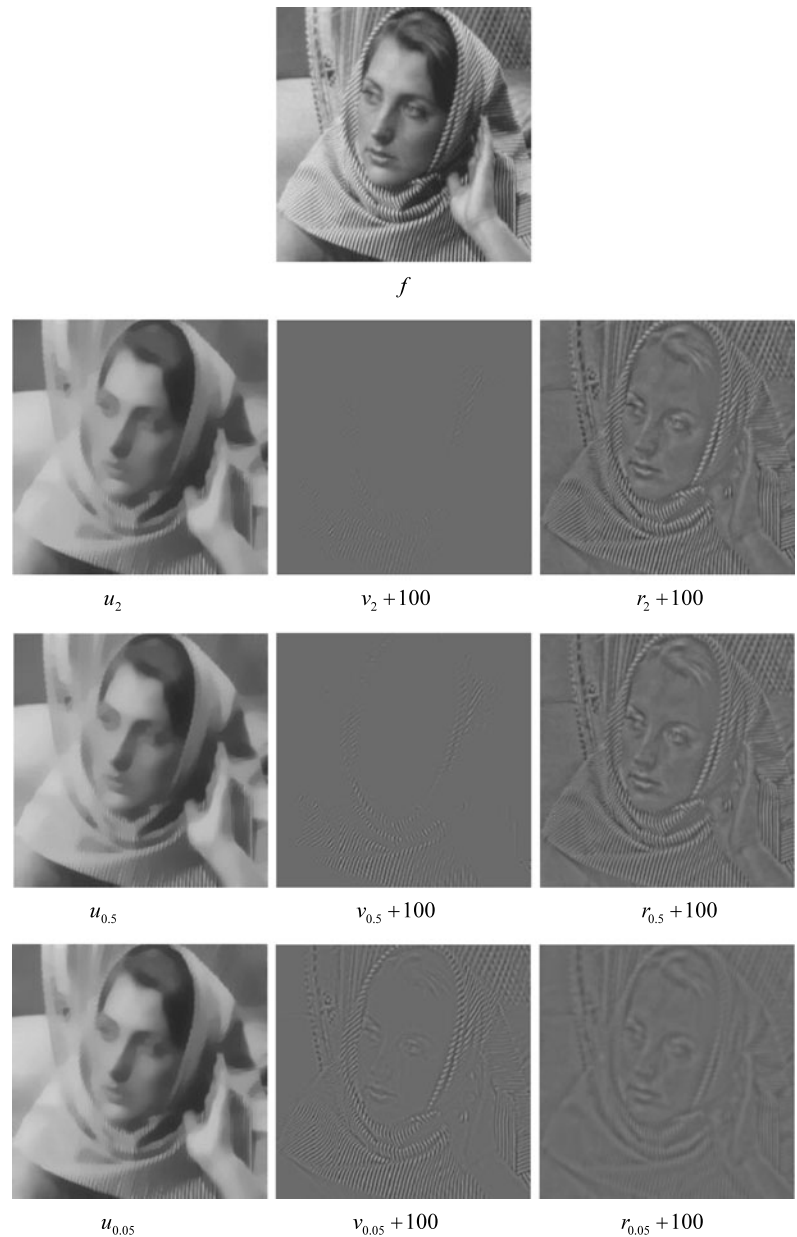
$$(u_{\lambda/2}, v_{\lambda/2}) = \arg \inf E(r_\lambda, \lambda/2; u, v). \tag{3}$$

We now have a better two-scale representation of texture given by  $v_\lambda + v_{\lambda/2}$ . Similarly, textures above scale  $2/\lambda$  remains unresolved in  $r_{\lambda/2}$ . Then, the process in (3) can be continued to capture larger scale textures. Starting with an initial scale  $\lambda = \lambda_0$ , we obtain

$$f = u_0 + v_0 + r_0,$$

here,

**Fig. 1** Here  $f$  is a given image.  $u_\lambda, v_\lambda$  and  $r_\lambda$  are structure, texture and residual component of  $f$ , respectively. The *first row* shows the decomposition  $f = u_2 + v_2 + r_2$  obtained by (2) with  $\lambda = 2$ . The *second row* shows the decomposition  $f = u_{0.5} + v_{0.5} + r_{0.5}$  obtained by (2) with  $\lambda = 0.5$ . The *last row* shows the decomposition obtained by (2) with  $\lambda = 0.05$ . In all decompositions, we take  $\mu = 0.005$



$$(u_0, v_0) = \arg \inf \{ E(f, \lambda_0; u, v) = |u|_{BV} + \mu \|f - u - v\|_{L^2}^2 + \lambda_0 \|v\|_{G_p} \}.$$

We proceed with successive application of a refinement step (3), it realizes as following,

$$r_i = u_{i+1} + v_{i+1} + r_{i+1}, \quad i = 0, 1, 2, \dots,$$

here,

$$(u_{i+1}, v_{i+1}) = \arg \inf \{ E(r_i, \lambda_0/2^{i+1}; u, v) = |u|_{BV} + \mu \|r_i - u - v\|_{L^2}^2 + \lambda_0/2^{i+1} \|v\|_{G_p} \}.$$

After  $k$  such steps, we can obtain the following hierarchical decomposition of  $f$ :

$$\begin{aligned} f &= u_0 + v_0 + r_0 \\ &= u_0 + u_1 + v_0 + v_1 + r_1 \\ &= \dots \\ &= u_0 + u_1 + \dots + u_k + v_0 + v_1 + \dots + v_k + r_k. \end{aligned} \tag{4}$$

#### 4 Some Properties of the Hierarchical $(BV, G_p, L^2)$ Decomposition

We recall that the hierarchical decomposition of a given image  $f \in L^2$  is achieved successively by solving the follow-

ing variational problem:

$$\inf_{u,v} \{ E(r_i, \lambda_0/2^{i+1}; u, v) \\ = J(u) + \mu \|r_i - u - v\|_{L^2}^2 + \lambda_0/2^{i+1} L(v) \}, \\ (i = -1, 0, 1, \dots), \tag{5}$$

where  $J(u) = |u|_{BV}$  and  $L(v) = \|v\|_{G_p}$  are two convex functions. We note here that  $r_i$  is the residual component of the  $(i + 1)$ th step decomposition and  $r_{-1}$  is interpreted as  $f$ , i.e.,  $r_{-1} = f$ . A natural way to solve the minimization problem (5) is to solve successively the following two coupled problems:

- Fixed  $v$ , find the solution  $u$  of

$$\inf_{u \in BV} \{ J(u) + \mu \|r_i - u - v\|_{L^2}^2 \}. \tag{6}$$

- Fixed  $u$ , find the solution  $v$  of

$$\inf_{v \in G_p} \{ \mu \|r_i - u - v\|_{L^2}^2 + \lambda_0/2^{i+1} L(v) \}. \tag{7}$$

Clearly, the problem (5) and the coupled problems (6)–(7) have the same solutions. In what follows, we will give some characteristics of their solutions.

Firstly, similar to (but slightly different from) Definition 5.3 of [27], we define a new quantity  $\|\cdot\|_{*,i}$  to measure the  $L^2$ -function, which will play key role in our following study.

**Definition 4** Given a function  $\omega \in L^2$  and an integral number  $i$ , define

$$\|\omega\|_{*,i} = \sup_{h \in BV, g \in G_p} \frac{\langle \omega, h + g \rangle}{|h|_{BV} + \lambda_0/2^{i+1} \|g\|_{G_p}}, \\ |h|_{BV} + \lambda_0/2^{i+1} \|g\|_{G_p} \neq 0,$$

where  $\langle \cdot, \cdot \rangle$  denotes  $L^2$  inner product.

*Remark 2* If  $\|\omega\|_{*,i} < \infty$ , then  $\int_{\Omega} \omega dx = 0$ ; otherwise, we can replace  $h$  by  $h + c$  with  $c \in \mathbb{R}$ , and then  $\|\omega\|_{*,i} = \infty$  as  $|c| \rightarrow \infty$ .

**Proposition 1** Let  $(u_{i+1}, v_{i+1})$  be a solution of (5) and set  $r_{i+1} = r_i - u_{i+1} - v_{i+1}$ , then we have the following:

- (1) If  $u_{i+1} = 0, v_{i+1} = 0$ , then  $\|r_i\|_{*,i} \leq \frac{1}{2\mu}$ .
- (2) If  $\|r_i\|_{*,i} > \frac{1}{2\mu}$ , then  $u_{i+1} \neq 0$  or  $v_{i+1} \neq 0$ . In addition,  $u_{i+1}, v_{i+1}$  and  $r_{i+1}$  satisfy

$$\|r_{i+1}\|_{*,i} = \frac{1}{2\mu} \quad \text{and} \\ \langle r_{i+1}, u_{i+1} + v_{i+1} \rangle \\ = \frac{1}{2\mu} (|u_{i+1}|_{BV} + \lambda_0/2^{i+1} \|v_{i+1}\|_{G_p}). \tag{8}$$

*Proof* For the first assertion, the model (5) yields  $u_{i+1} = 0, v_{i+1} = 0$  being the minimizer if and only if for any  $h \in BV$  and  $g \in G_p$ ,

$$|h|_{BV} + \mu \|r_i - h - g\|_{L^2}^2 + \lambda_0/2^{i+1} \|g\|_{G_p} \geq \mu \|r_i\|_{L^2}^2. \tag{9}$$

Expanding the second term of the left side of (9), we obtain

$$|h|_{BV} + \mu \|h + g\|_{L^2}^2 + \lambda_0/2^{i+1} \|g\|_{G_p} \geq 2\mu \langle r_i, h + g \rangle. \tag{10}$$

By substituting in (10)  $h$  with  $\varepsilon h$  and  $g$  with  $\varepsilon g$ , and taking  $\varepsilon \rightarrow 0^+$ , we have

$$\langle r_i, h + g \rangle \leq \frac{1}{2\mu} (|h|_{BV} + \lambda_0/2^{i+1} \|g\|_{G_p}).$$

By the definition of  $\|\cdot\|_{*,i}$ , we have  $\|r_i\|_{*,i} \leq \frac{1}{2\mu}$ .

For the second assertion, from the first assertion of this proposition, we can deduce directly that if  $\|r_i\|_{*,i} > \frac{1}{2\mu}$ , then  $u_{i+1} \neq 0$  or  $v_{i+1} \neq 0$ .

Since  $u_{i+1} \in BV$  and  $v_{i+1} \in G_p$  is the solution of (5), for any  $h \in BV, g \in G_p$  and  $\varepsilon \in \mathbb{R}$ , we have

$$E(r_i, \lambda_0/2^{i+1}; u_{i+1} + \varepsilon h, v_{i+1} + \varepsilon g) \\ \geq E(r_i, \lambda_0/2^{i+1}; u_{i+1}, v_{i+1})$$

which implies

$$\|u_{i+1} + \varepsilon h\|_{BV} + \mu \|r_{i+1} - \varepsilon(h + g)\|_{L^2}^2 \\ + \lambda_0/2^{i+1} \|v_{i+1} + \varepsilon g\|_{G_p} \\ \geq |u_{i+1}|_{BV} + \mu \|r_{i+1}\|_{L^2}^2 + \lambda_0/2^{i+1} \|v_{i+1}\|_{G_p}. \tag{11}$$

By the triangle inequality,

$$\|v_{i+1}\|_{G_p} + |\varepsilon| \|r_{i+1}\|_{G_p} \geq \|v_{i+1} + \varepsilon r_{i+1}\|_{G_p} \quad \text{and} \\ |u_{i+1} + \varepsilon h|_{BV} \geq |u_{i+1}|_{BV} + |\varepsilon| |h|_{BV}$$

equation (11) can be rewritten as

$$|\varepsilon| |h|_{BV} + \mu \|r_{i+1} - \varepsilon(h + g)\|_{L^2}^2 + \lambda_0/2^{i+1} |\varepsilon| \|g\|_{G_p} \\ \geq \mu \|r_{i+1}\|_{L^2}^2.$$

Expanding the last inequality, we obtain

$$|\varepsilon| |h|_{BV} + \mu \varepsilon^2 \|(h + g)\|_{L^2}^2 + \lambda_0/2^{i+1} |\varepsilon| \|g\|_{G_p} \\ \geq 2\varepsilon \mu \langle r_{i+1}, h + g \rangle.$$

Dividing both side of the last equation by  $\varepsilon > 0$ , and taking  $\varepsilon \rightarrow 0^+$ , we obtain

$$|h|_{BV} + \lambda_0/2^{i+1} \|g\|_{G_p} \geq 2\mu \langle r_{i+1}, h + g \rangle.$$

Therefore, by the definition of  $\|\cdot\|_{*,i}$  and the arbitrariness of  $h$  and  $g$ , we have

$$\|r_{i+1}\|_{*,i} \leq \frac{1}{2\mu}. \tag{12}$$

If we take  $\varepsilon \in (-1, 1)$ , and replace  $(h, g)$  with  $(u_{i+1}, v_{i+1})$  in (11), we have

$$\begin{aligned} (1 + \varepsilon)|u_{i+1}|_{BV} + \mu\|r_{i+1} - \varepsilon(u_{i+1} + v_{i+1})\|_{L^2}^2 \\ + \lambda_0/2^{i+1}(1 + \varepsilon)\|v_{i+1}\|_{G_p} \\ \geq |u_{i+1}|_{BV} + \mu\|r_{i+1}\|_{L^2}^2 + \lambda_0/2^{i+1}\|v_{i+1}\|_{G_p} \end{aligned}$$

which implies

$$\begin{aligned} \varepsilon|u_{i+1}|_{BV} + \mu\|r_{i+1} - \varepsilon(u_{i+1} + v_{i+1})\|_{L^2}^2 \\ + \lambda_0/2^{i+1}\varepsilon\|v_{i+1}\|_{G_p} \geq \mu\|r_{i+1}\|_{L^2}^2. \end{aligned}$$

By expanding the second term of right side of the last inequality, we have

$$\begin{aligned} \varepsilon|u_{i+1}|_{BV} + \varepsilon^2\mu\|u_{i+1} + v_{i+1}\|_{L^2}^2 + \varepsilon\lambda_0/2^{i+1}\|v_{i+1}\|_{G_p} \\ \geq 2\varepsilon\mu\langle r_{i+1}, u_{i+1} + v_{i+1} \rangle. \end{aligned} \tag{13}$$

If  $\varepsilon > 0$ , dividing both side of (13) by  $\varepsilon$  and then taking  $\varepsilon \rightarrow 0^+$ , we obtain

$$\begin{aligned} |u_{i+1}|_{BV} + \lambda_0/2^{i+1}\|v_{i+1}\|_{G_p} \\ \geq 2\mu\langle r_{i+1}, u_{i+1} + v_{i+1} \rangle. \end{aligned} \tag{14}$$

If  $\varepsilon < 0$ , similarly, we obtain

$$\begin{aligned} |u_{i+1}|_{BV} + \lambda_0/2^{i+1}\|v_{i+1}\|_{G_p} \\ \leq 2\mu\langle r_{i+1}, u_{i+1} + v_{i+1} \rangle. \end{aligned} \tag{15}$$

Therefore, from (14) and (15), we have desired result

$$\langle r_{i+1}, u_{i+1} + v_{i+1} \rangle = \frac{1}{2\mu}(|u_{i+1}|_{BV} + \lambda_0/2^{i+1}\|v_{i+1}\|_{G_p}).$$

Because  $u_{i+1} \neq 0$  or  $v_{i+1} \neq 0$ , the last equality can be rewritten as

$$\frac{\langle r_{i+1}, u_{i+1} + v_{i+1} \rangle}{|u_{i+1}|_{BV} + \lambda_0/2^{i+1}\|v_{i+1}\|_{G_p}} = \frac{1}{2\mu}. \tag{16}$$

Combining (12) with (16), we have

$$\|r_{i+1}\|_{*,i} = \frac{\langle r_{i+1}, u_{i+1} + v_{i+1} \rangle}{|u_{i+1}|_{BV} + \lambda_0/2^{i+1}\|v_{i+1}\|_{G_p}} = \frac{1}{2\mu}. \quad \square$$

Proposition 1 shows the characteristics of the solution of (5). We refer the reader to Meyer [34] for a similar one to the classical ROF decomposition [43] with the fixed parameter. From this proposition, we have the following result

of the nontrivial property of our hierarchical decomposition given in (4).

**Proposition 2** *If  $\int_{\Omega} f dx \neq 0$ , then the hierarchical decomposition given in (4) is nontrivial, i.e.,  $u_i \neq 0$  or  $v_i \neq 0$  for any  $i = 0, 1, \dots$*

*Proof* Because of  $\int_{\Omega} f dx \neq 0$ , we have  $\|f\|_{*, -1} = \|r_{-1}\|_{*, -1} > \frac{1}{2\mu}$  by Remark 2, which implies that the first step decomposition satisfies  $u_0 \neq 0$  or  $v_0 \neq 0$  by Proposition 1. In addition,

$$\|r_0\|_{*, -1} = \frac{\langle r_0, u_0 + v_0 \rangle}{|u_0|_{BV} + \lambda_0\|v_0\|_{G_p}} = \frac{1}{2\mu} \text{ and}$$

$$\|r_0\|_{*, 0} = \sup_{h \in BV, g \in G_p} \frac{\langle r_0, h + g \rangle}{|h|_{BV} + \lambda_0/2\|g\|_{G_p}},$$

which mean that the residual  $r_0$ , which will be the input data of the second step decomposition, satisfies

$$\|r_0\|_{*, 0} > \|r_0\|_{*, -1} = \frac{1}{2\mu}.$$

Again by Proposition 1, it follows that  $u_1 \neq 0$  or  $v_1 \neq 0$ , and  $\|r_1\|_{*, 1} > \|r_1\|_{*, 0} = \frac{1}{2\mu}$  which implies that the nontrivial decomposition can be continued.

Similarly, for the  $(i + 1)$ th step decomposition, the residual  $r_{i-1}$  of the previous step satisfies  $\|r_{i-1}\|_{*, i-1} > \|r_{i-1}\|_{*, i-2} = \frac{1}{2\mu}$ . So, by Proposition 1, we have  $u_i \neq 0$  or  $v_i \neq 0$ .  $\square$

From Proposition 2, we can conclude that if the initial image  $f$  satisfies  $\int_{\Omega} f dx \neq 0$ , then the hierarchical decomposition satisfies  $u_i \neq 0$  or  $v_i \neq 0$  for any  $i = 0, 1, \dots$ . In other word, if the first step decomposition is nontrivial, then the successive hierarchical decomposition is also nontrivial.

Next, we give the characteristics of the solutions of the coupled problems (6)–(7).

**Lemma 2** *Let  $(u_{i+1}, v_{i+1})$  be a solution of the coupled problems (6)–(7), then  $r_{i+1} = r_i - u_{i+1} - v_{i+1}$  is a solution of the following minimization problem:*

$$\inf_r \|r_i - v_{i+1} - r\|_{L^2}^2 \quad \text{subject to} \quad \|r\|_G \leq \frac{1}{2\mu}.$$

*Proof* Let  $v = v_{i+1}$  in (6), then  $u_{i+1}$  is a solution of (6) if and only if

$$0 \in \partial J(u_{i+1}) + 2\mu(u_{i+1} + v_{i+1} - r_i),$$

i.e.,

$$2\mu(r_i - u_{i+1} - v_{i+1}) \in \partial J(u_{i+1}), \tag{17}$$

where  $\partial J(u_{i+1})$  is the subdifferential of  $J$  at the point  $u_{i+1}$ ;  $\omega \in \partial J(u_{i+1})$  if and only if  $J(u) - J(u_{i+1}) \geq \langle \omega, u - u_{i+1} \rangle$  for every  $u \in BV$ . Euler-Lagrange equation (17) can be rewritten as

$$u_{i+1} \in \partial J^*(2\mu(r_i - u_{i+1} - v_{i+1})), \tag{18}$$

where  $J^*$  is the Legendre-Fenchel transform of  $J$ . Since  $J(u) = |u|_{BV}$  is one homogeneous (i.e.,  $J(\lambda u) = \lambda J(u)$  for any  $u \in BV$  and  $\lambda > 0$ ), it is well known that  $J^*$  is the indicator function of a closed convex set  $K' = \{v \mid \|v\|_G \leq 1\}$ , where  $J^*$  is defined as

$$J^*(v) = \sup_u \{ \langle v, u \rangle - J(u) \} = \chi_{K'}(v) = \begin{cases} 0 & \text{if } v \in K', \\ +\infty & \text{otherwise.} \end{cases} \tag{19}$$

Equation (18) can be rewritten as

$$0 \in r_i - u_{i+1} - v_{i+1} - r_i + v_{i+1} + \partial J^*(2\mu(r_i - u_{i+1} - v_{i+1})),$$

which precisely means that  $r_{i+1} = r_i - u_{i+1} - v_{i+1}$  is a solution of

$$\inf_r \left\{ \frac{1}{2} \|r_i - v_{i+1} - r\|_{L^2}^2 + \frac{1}{2\mu} J^*(2\mu r) \right\}.$$

By the definition of  $J^*$  given by (19),  $r_{i+1}$  is a solution of

$$\inf_{\|r\|_G \leq 1/(2\mu)} \|r_i - v_{i+1} - r\|_{L^2}^2. \tag{20}$$

We thus obtain the desired result. □

*Remark 3* Minimization problem (20) is actually a dual form of problem (6). By using the Euclidean projection algorithm proposed by Chambolle in [12], the solution of (20) can be written as  $r_{i+1} = P_{K'_\mu}(r_i - v_{i+1})$  which is just the orthogonal projection on the closed set  $K'_\mu$ , where  $K'_\mu = \{r \mid \|r\|_G \leq 1/(2\mu)\}$ .

By Lemma 2, we have the following result.

**Proposition 3** *Let  $(u_{i+1}, v_{i+1})$  be a solution of the coupled problems (6)–(7), then  $u_{i+1}, v_{i+1}$  and  $r_{i+1}$  satisfy the following:*

- (1) *If  $\|r_i - v_{i+1}\|_G \leq \frac{1}{2\mu}$ , then  $\|r_{i+1}\|_G \leq \frac{1}{2\mu}$  and  $u_{i+1} = 0$ .*
- (2) *If  $\|r_i - v_{i+1}\|_G > \frac{1}{2\mu}$ , then  $\|r_{i+1}\|_G = \frac{1}{2\mu}$  and  $u_{i+1} \neq 0$ .*

*Proof* For the first assertion, because of  $\|r_i - v_{i+1}\|_G \leq \frac{1}{2\mu}$ , we can deduce that  $r_i - v_{i+1} \in K'_\mu$ , and then  $r_i - v_{i+1} = P_{K'_\mu}(r_i - v_{i+1})$ . By Remark 3,  $r_{i+1} = P_{K'_\mu}(r_i - v_{i+1})$ . We thus have  $r_{i+1} = r_i - v_{i+1}$  which implies that  $\|r_{i+1}\|_G \leq \frac{1}{2\mu}$  and  $u_{i+1} = r_i - v_{i+1} - r_{i+1} = 0$ .

For the second assertion, because of  $\|r_i - v_{i+1}\|_G > \frac{1}{2\mu}$  and  $r_{i+1} = P_{K'_\mu}(r_i - v_{i+1})$ , on the basis of convex optimization theory, we have  $\|r_{i+1}\|_G = \frac{1}{2\mu}$ . Using the triangle inequality, we have

$$\|r_i - v_{i+1} - r_{i+1}\|_G \geq \|r_i - v_{i+1}\|_G - \|r_{i+1}\|_G > 0,$$

which means that  $u_{i+1} = r_i - v_{i+1} - r_{i+1} \neq 0$ . □

Next, we show another characteristic of the solution of the coupled problems (6)–(7) which is much related to texture extraction. We first need the following lemma.

**Lemma 3** *Let  $(u_{i+1}, v_{i+1})$  be a solution of the problems (6)–(7). Then  $r_{i+1} = r_i - u_{i+1} - v_{i+1}$  is a solution of the following minimization problem:*

$$\inf_r \|r_i - u_{i+1} - r\|_{L^2}^2 \quad \text{subject to} \quad \|\nabla r\|_{L^q} \leq \frac{\lambda_0}{2^{i+2}\mu},$$

where

$$\|\nabla r\|_{L^q} = \left( \int_\Omega |\nabla r|^q \right)^{1/q} \quad \text{and}$$

$$|\nabla r| = \sqrt{(\partial_x r)^2 + (\partial_y r)^2}.$$

*Proof* Fixed  $u = u_{i+1}$  in (7), we obtain that  $v_{i+1}$  is a solution of (7) if and only if

$$0 \in 2\mu(u_{i+1} + v_{i+1} - r_i) + \lambda_0/2^{i+1} \partial L(v_{i+1}),$$

i.e.,

$$\frac{2^{i+2}\mu}{\lambda_0}(r_i - u_{i+1} - v_{i+1}) \in \partial L(v_{i+1}), \tag{21}$$

where  $\partial L(v_{i+1})$  is subdifferential of  $L$  at  $v_{i+1}$ . Euler-Lagrange equation (21) can be rewritten as

$$v_{i+1} \in \partial L^* \left( \frac{2^{i+2}\mu}{\lambda_0}(r_i - u_{i+1} - v_{i+1}) \right), \tag{22}$$

where  $L^*$  is the Legendre-Fenchel transform of  $L$ , given by

$$L^*(u) = \chi_{K''}(u) = \begin{cases} 0 & \text{if } u \in K'', \\ +\infty & \text{otherwise} \end{cases} \tag{23}$$

with  $K'' = \{u \mid \|\nabla u\|_{L^q} \leq 1\}$ .

Equation (22) can be rewritten as

$$0 \in r_i - u_{i+1} - v_{i+1} - r_i + u_{i+1} + \partial L^* \left( \frac{2^{i+2}\mu}{\lambda_0}(r_i - u_{i+1} - v_{i+1}) \right),$$

which implies that  $r_{i+1} = r_i - u_{i+1} - v_{i+1}$  is a solution of

$$\inf_r \left\{ \frac{1}{2} \|r_i - u_{i+1} - r\|_{L^2}^2 + \frac{\lambda_0}{2^{i+2}\mu} L^* \left( \frac{2^{i+2}\mu}{\lambda_0} r \right) \right\}.$$

By the definition of  $L^*$  given in (23),  $r_{i+1}$  is a solution of the following problem

$$\inf_r \|r_i - u_{i+1} - r\|_{L^2}^2 \quad \text{subject to} \quad \|\nabla r\|_{L^q} \leq \frac{\lambda_0}{2^{i+2}\mu}. \quad (24)$$

We thus obtain the desired result. □

*Remark 4* Similar to Remark 3, the minimization problem (24) is a dual form of problem (7) and the solution of (24) can be written as  $r_{i+1} = P_{K'_\lambda}(r_i - u_{i+1})$ , the orthogonal projection on the closed set  $K'_\lambda = \{r \mid \|\nabla r\|_{L^q} \leq \lambda_0/(2^{i+2}\mu)\}$ .

By Lemma 3, we have the following result.

**Proposition 4** *Let  $(u_{i+1}, v_{i+1})$  be a solution of the coupled problems (6)–(7), then  $u_{i+1}, v_{i+1}$  and  $r_{i+1}$  satisfy the following:*

- (1) *If  $\|\nabla(r_i - u_{i+1})\|_{L^q} \leq \frac{\lambda_0}{2^{i+2}\mu}$ , then  $\|\nabla r_{i+1}\|_{L^q} \leq \frac{\lambda_0}{2^{i+2}\mu}$  and  $v_{i+1} = 0$ .*
- (2) *If  $\|\nabla(r_i - u_{i+1})\|_{L^q} > \frac{\lambda_0}{2^{i+2}\mu}$ , then  $\|\nabla r_{i+1}\|_{L^q} = \frac{\lambda_0}{2^{i+2}\mu}$  and  $v_{i+1} \neq 0$ .*

*Proof* These two assertions can be verified by the similar methods to the ones for Proposition 3. □

This proposition gives the conditions, under which texture can/cannot be effectively extracted by the hierarchical decomposition. Besides, it shows that the  $L^q$ -norm of  $|\nabla r_{i+1}|$  is decreasing with respect to  $i$ , which indicates that the residual component  $r_{i+1}$  contains less and less image information with the increase of the value of  $i$ . Further, we have the following convergence of the residual component.

**Proposition 5** *Let  $(u_{i+1}, v_{i+1})$  be a solution of (6)–(7), and  $r_{i+1} = r_i - u_{i+1} - v_{i+1}$ . Then  $r_{i+1} \rightarrow C$  as  $i \rightarrow \infty$ , where  $C$  is a constant.*

*Proof* By Proposition 4, in each case, we have

$$\|\nabla r_{i+1}\|_{L^q} = \left( \int_\Omega |\nabla r_{i+1}|^q \right)^{1/q} \leq \frac{\lambda_0}{2^{i+2}\mu} \rightarrow 0 \quad \text{as } i \rightarrow \infty. \quad (25)$$

Because of  $|\nabla r_{i+1}| = \sqrt{(\partial_x r_{i+1})^2 + (\partial_y r_{i+1})^2} \geq 0$ , from (25) we can deduce that  $|\nabla r_{i+1}| \rightarrow 0$  as  $i \rightarrow \infty$ , which implies that  $r_{i+1} \rightarrow C$  as  $i \rightarrow \infty$ . □

At last, similar to the convergence result of hierarchical  $(BV, L^2)$  decomposition proposed by Tadmor, Nezzar and Vese [48], we show the convergence of our hierarchical  $(BV, G_p, L^2)$  decomposition given by (4) in  $L^2$  topology.

**Proposition 6** *Let  $f \in L^2$ . Then the hierarchical decomposition given by (4) satisfies*

$$\left\| f - \sum_{i=-1}^k (u_{i+1} + v_{i+1}) \right\|_{L^2} = \|r_{k+1}\|_{L^2} \rightarrow 0, \quad \text{as } k \rightarrow \infty.$$

*In addition, the following energy decomposition of  $f$  holds:*

$$\begin{aligned} \|f\|_{L^2}^2 &= \sum_{i=-1}^{\infty} \|u_{i+1} + v_{i+1}\|_{L^2}^2 \\ &\quad + \frac{1}{\mu} \sum_{i=-1}^{\infty} (|u_{i+1}|_{BV} + \lambda_0/2^{i+1} \|v_{i+1}\|_{G_p}). \end{aligned}$$

*Proof* For the first assertion, since  $u_{i+1} \in BV$  and  $v_{i+1} \in G_p$  is a solution of the variational problem (5), for any  $\varepsilon \in \mathbb{R}$ , we have

$$\begin{aligned} E(r_i, \lambda_0/2^{i+1}; u_{i+1}, v_{i+1} + \varepsilon r_{i+1}) \\ \geq E(r_i, \lambda_0/2^{i+1}; u_{i+1}, v_{i+1}), \end{aligned}$$

which implies

$$\begin{aligned} |u_{i+1}|_{BV} + \mu \|r_{i+1} - \varepsilon r_{i+1}\|_{L^2}^2 + \lambda_0/2^{i+1} \|v_{i+1} + \varepsilon r_{i+1}\|_{G_p} \\ \geq |u_{i+1}|_{BV} + \mu \|r_{i+1}\|_{L^2}^2 + \lambda_0/2^{i+1} \|v_{i+1}\|_{G_p}. \end{aligned}$$

By the triangle inequality, it follows that

$$\mu \|r_{i+1} - \varepsilon r_{i+1}\|_{L^2}^2 + \lambda_0/2^{i+1} |\varepsilon| \|r_{i+1}\|_{G_p} \geq \mu \|r_{i+1}\|_{L^2}^2. \quad (26)$$

By expanding the first term of (26), we have

$$\mu \varepsilon^2 \|r_{i+1}\|_{L^2}^2 + \lambda_0/2^{i+1} |\varepsilon| \|r_{i+1}\|_{G_p} \geq 2\mu \varepsilon \|r_{i+1}\|_{L^2}^2.$$

Dividing both sides of the last inequality by  $\varepsilon > 0$  and taking  $\varepsilon \rightarrow 0^+$ , we have

$$\|r_{i+1}\|_{L^2}^2 \leq \frac{\lambda_0}{2^{i+2}\mu} \|r_{i+1}\|_{G_p}.$$

From Remark 1 and Proposition 1, we have

$$\|r_{i+1}\|_{L^2}^2 \leq \frac{\lambda_0 C_\Omega}{2^{i+3}\mu^2}$$

which implies

$$\|r_{i+1}\|_{L^2} \rightarrow 0 \quad \text{as } i \rightarrow \infty.$$

Since  $r_{k+1} = f - \sum_{i=-1}^k (u_{i+1} + v_{i+1})$ , we have

$$\left\| f - \sum_{i=-1}^k (u_{i+1} + v_{i+1}) \right\|_{L^2} = \|r_{k+1}\|_{L^2} \rightarrow 0, \quad \text{as } k \rightarrow \infty.$$

For the second assertion, we begin by squaring the basic refinement step,

$$\begin{aligned} r_i &= u_{i+1} + v_{i+1} + r_{i+1} \\ \Rightarrow r_i &= r_{i+1} + (u_{i+1} + v_{i+1}), \quad i = -1, 0, 1, \dots \end{aligned}$$

Then, we can obtain

$$\|r_i\|_{L^2}^2 = \|r_{i+1}\|_{L^2}^2 + \|u_{i+1} + v_{i+1}\|_{L^2}^2 + 2\langle r_{i+1}, u_{i+1} + v_{i+1} \rangle. \tag{27}$$

Because  $(u_{i+1}, v_{i+1})$  is a solution of (5), by Proposition 1, (27) can be written as

$$\begin{aligned} \|r_i\|_{L^2}^2 - \|r_{i+1}\|_{L^2}^2 - \|u_{i+1} + v_{i+1}\|_{L^2}^2 &= 2\langle r_{i+1}, u_{i+1} + v_{i+1} \rangle \\ &= \frac{1}{\mu} (|u_{i+1}|_{BV} + \lambda_0/2^{i+1} \|v_{i+1}\|_{G_p}). \end{aligned} \tag{28}$$

Since

$$\begin{aligned} &\sum_{i=-1}^k (\|r_i\|_{L^2}^2 - \|r_{i+1}\|_{L^2}^2 - \|u_{i+1} + v_{i+1}\|_{L^2}^2) \\ &= \sum_{i=-1}^k (\|r_i\|_{L^2}^2 - \|r_{i+1}\|_{L^2}^2) - \sum_{i=-1}^k \|u_{i+1} + v_{i+1}\|_{L^2}^2 \\ &= \|r_{-1}\|_{L^2}^2 - \|r_{k+1}\|_{L^2}^2 - \sum_{i=-1}^k \|u_{i+1} + v_{i+1}\|_{L^2}^2 \\ &= \|f\|_{L^2}^2 - \|r_{k+1}\|_{L^2}^2 - \sum_{i=-1}^k \|u_{i+1} + v_{i+1}\|_{L^2}^2. \end{aligned}$$

Summing up (28), we have

$$\begin{aligned} \|f\|_{L^2}^2 &= \|r_{k+1}\|_{L^2}^2 + \sum_{i=-1}^k \|u_{i+1} + v_{i+1}\|_{L^2}^2 \\ &\quad + \frac{1}{\mu} \sum_{i=-1}^k (|u_{i+1}|_{BV} + \lambda_0/2^{i+1} \|v_{i+1}\|_{G_p}). \end{aligned}$$

Because  $\lim_{k \rightarrow \infty} \|r_{k+1}\|_{L^2} \rightarrow 0$ , we have

$$\|f\|_{L^2}^2 = \sum_{i=-1}^{\infty} \|u_{i+1} + v_{i+1}\|_{L^2}^2$$

$$+ \frac{1}{\mu} \sum_{i=-1}^{\infty} (|u_{i+1}|_{BV} + \lambda_0/2^{i+1} \|v_{i+1}\|_{G_p}). \quad \square$$

The last equation can be seen as the quadratic  $L^2$ -energy decomposition of  $f$  in our hierarchical decomposition given by (4). We refer the reader to Tadmor, Nezzar and Vese [48] for a similar one to hierarchical  $(BV, L^2)$  decomposition. Further, the multiscale nature of hierarchical texture extraction can be quantified in term of this energy decomposition.

### 5 Numerical Implementation

Because of  $v \in G_p$ , taking  $v = \text{div}(g_1, g_2)$ , we obtain an equivalent formulation of (5) in terms of  $u, g_1$  and  $g_2$ :

$$\begin{aligned} &\inf_{u, g_1, g_2} \left\{ |u|_{BV} + \mu \|r_k - u - \partial_x g_1 - \partial_y g_2\|_{L^2}^2 \right. \\ &\quad \left. + \lambda_0/2^{k+1} \left\| \sqrt{g_1^2 + g_2^2} \right\|_{L^p} \right\}, \\ &k = -1, 0, 1, \dots \end{aligned} \tag{29}$$

Note that in order not to cause the confusion of subscripts in what follows, the  $i$  in (5) is replaced by  $k$  in (29). Similarly, computing the minimizer of problem (29) amounts to solve the two following minimization problems:

- Fixed  $(g_1, g_2)$ , find the solution  $u$  of:
 
$$\inf_u \{ |u|_{BV} + \mu \|r_k - u - \partial_x g_1 - \partial_y g_2\|_{L^2}^2 \}. \tag{30}$$
- Fixed  $u$ , find the solution  $(g_1, g_2)$  of
 
$$\inf_{g_1, g_2} \left\{ \mu \|r_k - u - \partial_x g_1 - \partial_y g_2\|_{L^2}^2 \right. \\ \left. + \lambda_0/2^{k+1} \left\| \sqrt{g_1^2 + g_2^2} \right\|_{L^p} \right\}. \tag{31}$$

Minimization problem (30) is actually ROF model. We here adopt the projection algorithm in the dual framework proposed by Chambolle [12] to solve it. By Remark 2, the solution  $u_{k+1}$  can be written as

$$u_{k+1} = r_k - \partial_x g_1 - \partial_y g_2 - P_{K'_\mu}(r_k - \partial_x g_1 - \partial_y g_2),$$

where  $P_{K'_\mu}(r_k - \partial_x g_1 - \partial_y g_2)$  is the orthogonal projection of  $r_k - \partial_x g_1 - \partial_y g_2$  on the closed convex set  $K'_\mu = \{r \mid \|r\|_G \leq 1/(2\mu)\}$ . In the discrete setting, the computation of the non-linear projection  $P_{K'_\mu}(r_k - \partial_x g_1 - \partial_y g_2)$  amounts to solve the following constrained minimization problem with inequality constraints:

$$\begin{aligned} &\min_{\xi} \left\{ \|\text{div}(\xi) - 2\mu(r_k - \partial_x g_1 - \partial_y g_2)\|_{L^2}^2, \right. \\ &\quad \left. |\xi_{i,j}| \leq 1, \quad i = 1, \dots, M; \quad j = 1, \dots, N \right\}, \end{aligned} \tag{32}$$

where  $M \times N$  indicate the size of image and  $|\xi_{i,j}| = \sqrt{(\xi_{i,j}^1)^2 + (\xi_{i,j}^2)^2}$ . The Euler-Lagrange equation of (32) is

$$-\nabla(\operatorname{div}(\xi) - 2\mu(r_k - \partial_x g_1 - \partial_y g_2))_{i,j} + a_{i,j}\xi_{i,j} = 0 \quad (33)$$

where the  $a_{i,j}$ 's are the Lagrange multipliers associated to each constrain in problem (32). By the complementary slackness condition, we have either  $a_{i,j} > 0$  and  $|\xi_{i,j}| = 1$ , or  $|\xi_{i,j}| < 1$  and  $a_{i,j} = 0$ . In the latter case we also have  $\nabla(\operatorname{div}(\xi) - 2\mu(r_k - \partial_x g_1 - \partial_y g_2))_{i,j} = 0$ . So, in either case, the Lagrange multipliers are

$$a_{i,j} = |\nabla(\operatorname{div}(\xi) - 2\mu(r_k - \partial_x g_1 - \partial_y g_2))_{i,j}|.$$

Then, (33) can be solved by the following semi-implicit fixed point iteration scheme:

$$\begin{aligned} \xi_{i,j}^{n+1} &= \xi_{i,j}^n + \tau(\nabla(\operatorname{div}(\xi^n) - 2\mu(r_k - \partial_x g_1 - \partial_y g_2)))_{i,j} \\ &\quad - \tau a_{i,j}^n \xi_{i,j}^{n+1}. \end{aligned}$$

Solving  $\xi_{i,j}^{n+1}$  in the last equation, we obtain the final iteration scheme:

$$\begin{aligned} \xi^0 &= 0, \\ \xi_{i,j}^{n+1} &= \frac{\xi_{i,j}^n + \tau(\nabla(\operatorname{div}(\xi^n) - 2\mu(r_k - \partial_x g_1 - \partial_y g_2)))_{i,j}}{1 + \tau|\nabla(\operatorname{div}(\xi^n) - 2\mu(r_k - \partial_x g_1 - \partial_y g_2))_{i,j}|}. \end{aligned} \quad (34)$$

Here, the discrete version of the partial derivative predator  $(\partial_x g)_{i,j}$  and  $(\partial_y g)_{i,j}$  are defined as

$$\begin{aligned} (\partial_x g)_{i,j} &= \begin{cases} g_{i,j+1} - g_{i,j} & \text{if } j < N, \\ 0 & \text{if } j = N \end{cases} \quad \text{and} \\ (\partial_y g)_{i,j} &= \begin{cases} g_{i+1,j} - g_{i,j} & \text{if } i < M, \\ 0 & \text{if } i = M. \end{cases} \end{aligned} \quad (35)$$

The discrete version of the gradient predator  $(\nabla u)_{i,j} = ((\partial_x u)_{i,j}, (\partial_y u)_{i,j})$  is defined as

$$\begin{aligned} (\partial_x u)_{i,j} &= \begin{cases} u_{i,j+1} - u_{i,j} & \text{if } j < N, \\ 0 & \text{if } j = N \end{cases} \quad \text{and} \\ (\partial_y u)_{i,j} &= \begin{cases} u_{i+1,j} - u_{i,j} & \text{if } i < M, \\ 0 & \text{if } i = M. \end{cases} \end{aligned} \quad (36)$$

And the discrete version of the divergence predator  $(\operatorname{div}(\xi^1, \xi^2))_{i,j}$  is given by

$$\begin{aligned} (\operatorname{div}(\xi^1, \xi^2))_{i,j} &= \begin{cases} \xi_{i,j}^1 - \xi_{i,j-1}^1 & \text{if } 1 < j < N, \\ \xi_{i,j}^1 & \text{if } j = 1, \\ -\xi_{i,j-1}^1 & \text{if } j = N \end{cases} \\ &\quad + \begin{cases} \xi_{i,j}^2 - \xi_{i-1,j}^2 & \text{if } 1 < i < M, \\ \xi_{i,j}^2 & \text{if } i = 1, \\ -\xi_{i-1,j}^2 & \text{if } i = M. \end{cases} \end{aligned} \quad (37)$$

In [12], a sufficient condition was introduced to ensure the convergence of the iterative formula (34). This sufficient condition shows that as long as  $\tau \leq 1/8$ , then  $\frac{1}{2\mu} \operatorname{div}(\xi^n) \rightarrow P_{K'_\mu}(r_k - \partial_x g_1 - \partial_y g_2)$  as  $n \rightarrow +\infty$ .

Minimizing (31) with respect to  $g_1$  and  $g_2$  yields the following coupled Euler-Lagrange equations:

$$\begin{aligned} \lambda_0/2^{k+1} \left( \left\| \sqrt{g_1^2 + g_2^2} \right\|_{L^p} \right)^{1-p} \left( \sqrt{g_1^2 + g_2^2} \right)^{p-2} g_1 \\ = 2\mu \partial_x (u - r_k + \partial_x g_1 + \partial_y g_2), \end{aligned} \quad (38)$$

$$\begin{aligned} \lambda_0/2^{k+1} \left( \left\| \sqrt{g_1^2 + g_2^2} \right\|_{L^p} \right)^{1-p} \left( \sqrt{g_1^2 + g_2^2} \right)^{p-2} g_2 \\ = 2\mu \partial_y (u - r_k + \partial_x g_1 + \partial_y g_2). \end{aligned} \quad (39)$$

If the exterior normal to the boundary  $\partial\Omega$  is denoted by  $(n_x, n_y)$ , then the associated boundary conditions for  $g_1$  and  $g_2$  are:

$$\begin{aligned} (r_k - u - \partial_x g_1 - \partial_y g_2)n_x &= 0; \\ (r_k - u - \partial_x g_1 - \partial_y g_2)n_y &= 0. \end{aligned} \quad (40)$$

We use the alternating algorithm to solve the coupled equations (38)–(39) with the boundary conditions (40). In the discrete setting, for each equation, we use semi-implicit fixed point iteration scheme [51]. To simplify the presentation, we introduce the notation

$$H(g_1, g_2) = \left( \left\| \sqrt{g_1^2 + g_2^2} \right\|_{L^p} \right)^{1-p} \left( \sqrt{g_1^2 + g_2^2} \right)^{p-2}.$$

The alternating algorithm is presented as follows:

- Fixed  $g_2$ , update the value of  $g_1$  by

$$\begin{aligned} \lambda_0/2^{k+1} H_{i,j}^n g_{1,i,j}^{n+1} \\ = 2\mu((\partial_x(u - r_k))_{i,j}^n + g_{1,i,j+1}^n \\ - 2g_{1,i,j}^{n+1} + g_{1,i,j-1}^n + (\partial_{xy}^2 g_2)_{i,j}^n). \end{aligned} \quad (41)$$

- Fixed  $g_1$ , update the value of  $g_2$  by

$$\begin{aligned} \lambda_0/2^{k+1} H_{i,j}^n g_{2,i,j}^{n+1} \\ = 2\mu((\partial_y(u - r_k))_{i,j}^n + g_{2,i+1,j}^n \\ - 2g_{2,i,j}^{n+1} + g_{2,i-1,j}^n + (\partial_{xy}^2 g_1)_{i,j}^n). \end{aligned} \quad (42)$$

Here  $H_{i,j}^n = H(g_{1,i,j}^n, g_{2,i,j}^n)$ ,  $(\partial_x \cdot)_{i,j}$  and  $(\partial_y \cdot)_{i,j}$  is defined by (35) and the discrete version of the mixed second partial derivative predator  $(\partial_{xy}^2 g)_{i,j}$  is given by

$$(\partial_{xy}^2 g)_{i,j} = \begin{cases} 0 & \text{if } i = 1, M, j = 1, N, \\ \frac{1}{4}(g_{i+1,j+1} + g_{i-1,j-1} + g_{i+1,j-1} - g_{i-1,j+1}) & \text{if } 1 < i < M, 1 < j < N. \end{cases}$$

Solving (41)–(42) for  $g_{1,i,j}^{n+1}$  and  $g_{2,i,j}^{n+1}$ , respectively, we have

$$g_{1,i,j}^{n+1} = \frac{2\mu}{\lambda_0/2^{k+1}H_{i,j}^n + 4\mu} \times ((\partial_x(u - r_k))_{i,j}^n + g_{1,i,j+1}^n + g_{1,i,j-1}^n + (\partial_{xy}^2 g_2)_{i,j}^n),$$

$$g_{2,i,j}^{n+1} = \frac{2\mu}{\lambda_0/2^{k+1}H_{i,j}^n + 4\mu} \times ((\partial_y(u - r_k))_{i,j}^n + g_{2,i+1,j}^n + g_{2,i-1,j}^n + (\partial_{xy}^2 g_1)_{i,j}^n).$$

In practice, we always use the most recent values to compute the values of function at each point during iteration process.

The principal steps of the algorithm for the proposed model can be formulated as follows:

1. Initialize  $u^0 = g_1^0 = g_2^0 = 0$  and  $n = 0$ .
2. Compute  $\xi$ :
  - (1) Initialize  $\xi^0 = 0$  and  $n = 0$ .
  - (2) Compute  $\xi^{n+1}$  by

$$\xi_{i,j}^{n+1} = \frac{\xi_{i,j}^n + \tau(\nabla(\text{div}(\xi^n) - 2\mu(r_k - \partial_x g_1^n - \partial_y g_2^n)))_{i,j}}{1 + \tau|\nabla(\text{div}(\xi^n) - 2\mu(r_k - \partial_x g_1^n - \partial_y g_2^n))_{i,j}|}.$$

- (3) Check whether  $|\text{div}(\xi_{i,j}^{n+1}) - \text{div}(\xi_{i,j}^n)| \leq \varepsilon$  holds. If not, set  $n = n + 1$  and go to step (2).
3. Compute  $u^{n+1}$  by

$$u_{i,j}^{n+1} = r_{k,i,j} - (\partial_x g_1)_{i,j}^n - (\partial_y g_2)_{i,j}^n - \frac{1}{2\mu} \text{div}(\xi_{i,j}^{n+1}).$$

4. Compute  $g_1^{n+1}$  by

$$g_{1,i,j}^{n+1} = \frac{2\mu}{\lambda_0/2^{k+1}H(g_{1,i,j}^n, g_{2,i,j}^n) + 4\mu} \times ((\partial_x(u - r_k))_{i,j}^{n+1} + g_{1,i,j+1}^n + g_{1,i,j-1}^n + (\partial_{xy}^2 g_2)_{i,j}^n).$$

5. Compute  $g_2^{n+1}$  by

$$g_{2,i,j}^{n+1} = \frac{2\mu}{\lambda_0/2^{k+1}H(g_{1,i,j}^{n+1}, g_{2,i,j}^n) + 4\mu} \times ((\partial_y(u - r_k))_{i,j}^{n+1} + g_{2,i+1,j}^n + g_{2,i-1,j}^n + (\partial_{xy}^2 g_1)_{i,j}^{n+1}).$$

6. Check whether  $\max\{|u^{n+1} - u^n|, |\text{div}(g_1^{n+1}, g_2^{n+1}) - \text{div}(g_1^n, g_2^n)|\} \leq \varepsilon$  holds. If not, set  $n = n + 1$  and go back to step 2.

### 6 Applications to Multiscale Texture Extraction

In this section, we apply the hierarchical  $(BV, G_p, L^2)$  decomposition presented in (4) to achieve a multiscale texture extraction. From (4), the multiscale texture representation of  $f$  can be presented as

$$\sum_{i=0}^k v_i = f - \sum_{i=0}^k u_i - r_k.$$

The construction of this multiscale texture extraction is independent of the priori parameter  $\lambda_0$ . And the partial sum,  $\sum_{i=0}^k v_i$  can provide a multi-layered description of texture which lies in an intermediate scale space between  $G_p$  and  $L^2$ . This multi-layered texture extraction can capture texture in the deferent scales. As  $k$  increases, the  $v_k$ 's will successively resolve textures with decreasing the value of the scale parameter  $\lambda_0/2^{k+1}$ . In addition, we note in passing that, as usual, coarser and finer extractions are available by using different ladders of scales, e.g.,  $\lambda_0/s^{k+1}$  with  $1 < s < 2$  (respectively  $s > 2$ ) leading to a finer (respectively coarser) texture extraction.

In what follows, synthetic textured images as well as real ones are used to test and validate the proposed approach for multiscale texture extraction. In all numerical experiments shown below, we choose the parameters as following:  $\mu = 0.005$ ,  $\lambda_0 = 2$  (initial scale parameter),  $\tau = 0.05$ . We have tested our model with different values of  $p$  and found results similar, while the case of  $p = 1$  yields faster calculations per iteration, which is identical with the conclusion in [51, 52]. Thus, similar to the selection of  $p$  in [51, 52], we set  $p = 1$  in the following experiments.

Figure 2 shows the results of multiscale texture extraction of a synthetic image for 7 steps. The first image shows the test data  $f$  and the next seven images show the ‘textures+100’ (plus a constant for illustration purposes) of  $f$  at different scales. We can clearly see that at first only coarsest texture has been extracted, while more and more smooth textures are extracted with the increase of the iteration times. The last plots show the  $G_p$ -energy of  $v_i$  and the  $L^2$ -energy of  $r_i$ , respectively.

**Fig. 2** Multiscale texture extraction of a synthetic image for 7 steps, and the two plots show the  $G_p$ -energy of texture  $v_i$  and the  $L^2$ -energy of residual  $r_i$ , respectively

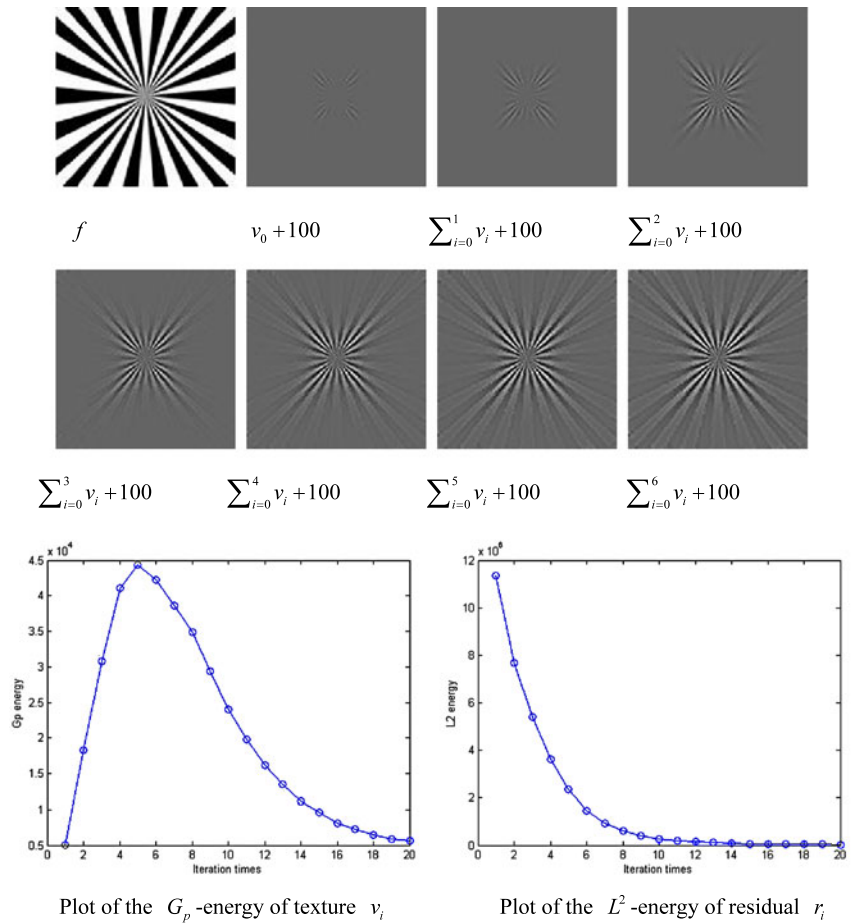


**Fig. 3** Multiscale texture extraction of a synthetic image for 7 steps

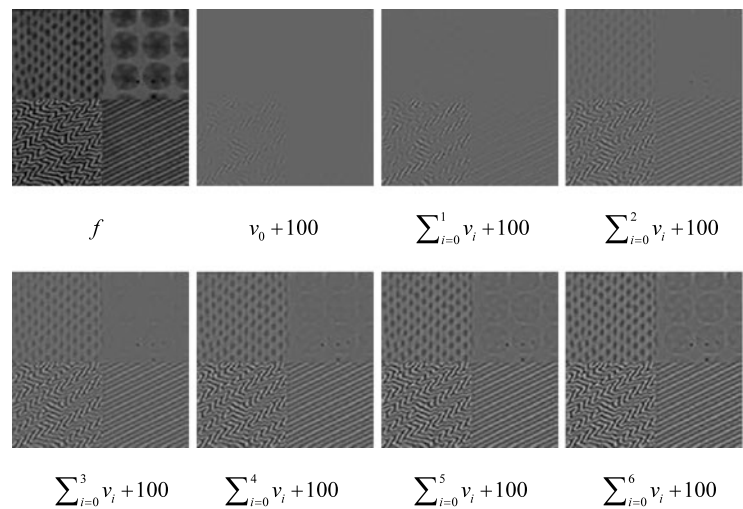


Figure 3 shows the results of multiscale texture extraction of another synthetic image for 7 steps. We get similar results and conclusions with the first experiment.

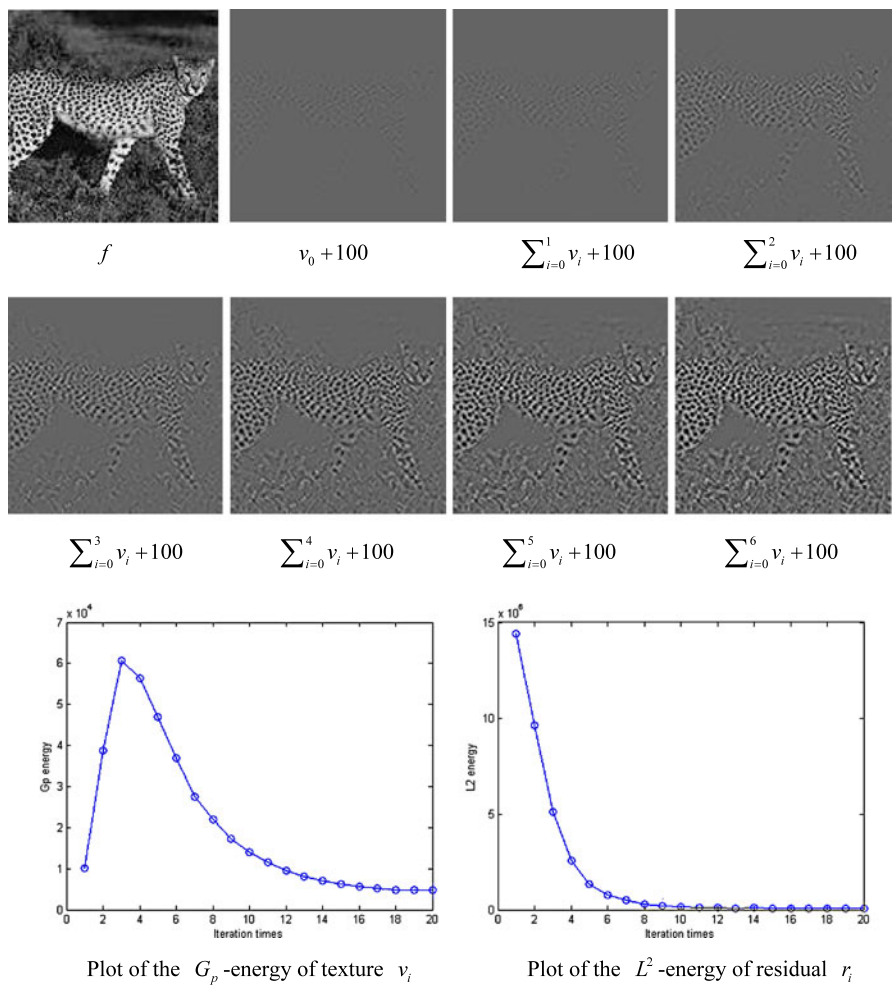
Figure 4 shows the results of multiscale texture extraction of a leopard image for 7 steps. The  $G_p$ -energy of  $v_i$  and the  $L^2$ -energy of residual  $r_i$  are also plotted in this figure.

Figure 5 shows the results of multiscale texture extraction of a fingerprint image for 7 steps.

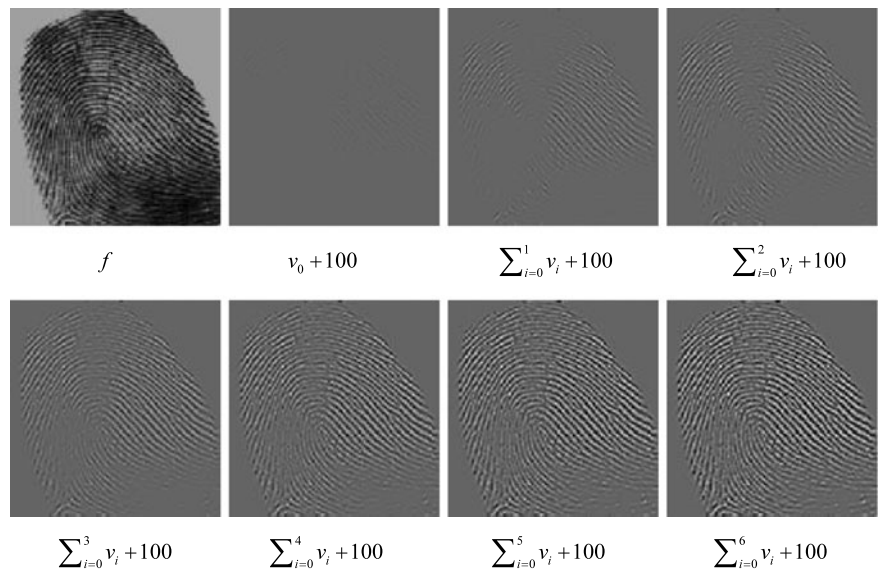
### 7 Conclusions

In this paper, we present a new multiscale texture extraction method which is distinct from all previous models of mul-

**Fig. 4** Multiscale texture extraction of a leopard image for 7 steps, and the two plots show the  $G_p$ -energy of  $v_i$  and the  $L^2$ -energy of residual  $r_i$ , respectively



**Fig. 5** Multiscale texture extraction of a fingerprint image for 7 steps



tiscale texture representation. Our method may have some limitations compared with the other classical models such as Gabor filter and wavelet transform, because we only take

into account the scales of texture, and ignore some other information such as direction and structure of texture. But we are the first one to represent the multiscale texture in

the variational framework. In the future, we will extend this method by taking into account more texture information.

## References

1. Abbadeni, N.: Texture representation and retrieval using the causal autoregressive model. *J. Vis. Commun. Image Represent.* **21**(7), 651–664 (2010)
2. Arunachalam, N., Ramamoorthy, B.: Fourier transform based texture measures for grinding wheel condition monitoring using machine vision. *Int. J. Manuf. Technol. Manag.* **21**, 112–121 (2010)
3. Ashish, B.K., Kumar, A., Padhy, P.K.: Satellite image processing using discrete cosine transform and singular value decomposition. *Adv. Digit. Image Process. Inf. Sci.* **205**(1), 277–290 (2011)
4. Aubert, G., Aujol, J.: Modeling very oscillating signals. Application to image processing. *Appl. Math. Optim.* **51**, 163–182 (2003)
5. Aubert, G., Kornprobst, P.: *Mathematical Problems in Image Processing*. Springer, New York (2001)
6. Aujol, J., Aubert, G., Blanc-Féraud, L., Chambolle, A.: Image decomposition application to SAR images. *Scale Space Methods Comput. Vis.* **2695**, 297–312 (2003)
7. Aujol, J., Aubert, G., Blanc-Féraud, L., Chambolle, A.: Image decomposition into a bounded variation component and an oscillating component. *J. Math. Imaging Vis.* **22**(1), 71–88 (2005)
8. Athavale, P., Tadmor, E.: Integro-differential equations based on  $(BV, L^1)$  image decomposition. *SIAM J. Imaging Sci.* **4**(1), 300–312 (2011)
9. Bovik, A.C., Clark, M., Geisler, W.S.: Multichannel texture analysis using localized spatial filters. *IEEE Trans. Pattern Anal. Mach. Intell.* **12**(1), 55–73 (1990)
10. Buades, A., Le, T., Morel, J., Vese, L.: Fast cartoon + texture image filters. *IEEE Trans. Image Process.* **19**, 1978–1986 (2010)
11. Cesmeli, E., Wang, D.L.: Texture segmentation using Gaussian Markov random fields and neural oscillator networks. *IEEE Trans. Neural Netw.* **12**(2), 394–404 (2001)
12. Chambolle, A.: An algorithm for total variation minimization and applications. *J. Math. Imaging Vis.* **20**, 89–97 (2004)
13. Chan, T., Shen, J., Vese, L.: Variational PDE models in image processing. *Not. Am. Math. Soc.* **50**, 14–26 (2003)
14. Chan, T., Esedoglua, S., Park, F.: Image decomposition combining staircase reduction and texture extraction. *J. Vis. Commun. Image Represent.* **18**, 464–486 (2007)
15. Chan, T., Esedoglua, S., Park, F.: Fourth order dual method for staircase reduction in texture extraction and image restoration problems. In: 17th IEEE International Conference on Image Processing (ICIP), 2010, vol. 26–29, pp. 4137–4140 (2010)
16. Chen, C.C., Daponte, J.S., Fox, M.D.: Fractal feature analysis and classification in medical imaging. *IEEE Trans. Med. Imaging* **8**(2), 133–142 (1989)
17. Coburn, C.A., Roberts, A.C.B.: A multiscale texture analysis procedure for improved forest stand classification. *Int. J. Remote Sens.* **25**(20), 4287–4308 (2004)
18. Daugman, J.: Complete discrete 2D Gabor transform by neural networks for image analysis and compression. *IEEE Trans. Acoust. Speech Signal Process.* **36**, 1169–1179 (1988)
19. Fauzi, M.F.A., Lewis, P.H.: A multiscale approach to texture-based image retrieval. *PAA Pattern Anal. Appl.* **11**, 141–157 (2008)
20. Gimelfarb, G.: *Image Textures and Gibbs Random Fields*. Kluwer Academic, Dordrecht (1999)
21. Haralick, R.M.: Statistical and structural approaches to texture. *Proc. IEEE* **67**(5), 786–804 (1979)
22. Haralick, R.M., Shanmugam, K., Dinstein, I.: Textural features for image classification. *IEEE Trans. Syst. Man Cybern.* **3**(6), 610–621 (1973)
23. Hay, G.J., Niemann, K.O.: Visualizing 3-D texture: A three-dimensional structural approach to model forest texture. *Can. J. Remote Sens.* **20**, 90–101 (1994)
24. Hormigo, J., Cristobal, G.: High resolution spectral analysis of images using the pseudo-Wigner distribution. *IEEE Trans. Signal Process.* **46**(6), 1757–1763 (1998)
25. Jain, A.K., Farrokhnia, F.: Unsupervised texture segmentation using Gabor filters. *Pattern Recognit.* **24**(12), 1167–1186 (1991)
26. Julesz, B., Bergen, J.R.: Textons, the fundamental elements in preattentive vision and perception of textures. *Bell Syst. Tech. J.* **62**(6), 1619–1645 (1983)
27. Le, T., Vese, L.: Image decomposition using total variation and div(BMO). *Multiscale Model. Simul.* **4**, 390–423 (2005)
28. Liang, K.H., Tjahjadi, T.: Adaptive scale fixing for multiscale texture segmentation. *IEEE Trans. Image Process.* **15**(1), 249–256 (2006)
29. Liu, X., Wang, D.: Texture classification using spectral histograms. *IEEE Trans. Image Process.* **12**(6), 661–670 (2003)
30. Mallat, S.: Wavelets for a vision. *Proc. IEEE* **84**(4), 604–614 (1996)
31. Mao, J.C., Jain, A.K.: Texture classification and segmentation using multi-resolution simultaneous autoregressive models. *Pattern Recognit.* **25**(2), 173–188 (1992)
32. Materka, A., Strzelecki, M.: *Texture analysis methods—a review*. COST B11 report, Technical University of Lodz (1998)
33. Meyer, Y.: *Wavelets: Algorithms and Applications*. SIAM, Philadelphia (1993)
34. Meyer, Y.: Oscillating patterns in image processing and nonlinear evolution equations. In: *Univ. Lecture Ser.*, vol. 22. AMS, Providence (2001)
35. Michael, D.: Wavelet features for color image classification. In: *Annual Conference Imaging and Geospatial Information Society*, Orlando (2000)
36. Nesterov, Y.: Smooth minimization of non-smooth functions. *Math. Program., Ser. A* **103**, 127–152 (2005)
37. Nunes, J.C., Guyot, S., Delechelle, E.: Texture analysis based on local analysis of the bidimensional empirical mode decomposition. *Mach. Vis. Appl.* **16**, 177–188 (2005)
38. Osher, S., Solé, A., Vese, L.: Image decomposition and restoration using total variation minimization and the  $H^{-1}$  norm. *Multiscale Model. Simul.* **1**(3), 349–370 (2003)
39. Pentland, A.P.: Fractal-based description of natural scenes. *IEEE Trans. Pattern Anal. Mach. Intell.* **6**, 661–674 (1984)
40. Pichler, O., Teuner, A., Hosticka, B.J.: A comparison of texture feature extraction using adaptive Gabor filtering pyramidal and tree structured wavelet transforms. *Pattern Recognit.* **29**(5), 733–742 (1996)
41. Pu, Y.F., Zhou, J.L.: A novel approach for multi-scale texture segmentation based on fractional differential. *Int. J. Comput. Math.* **88**(1), 58–78 (2011)
42. Reed, T.R., Wechsler, H.: Segmentation of textured images and Gestalt organization using spatial/spatial-frequency representations. *IEEE Trans. Pattern Anal. Mach. Intell.* **12**, 1–12 (1990)
43. Rudin, L., Osher, S., Fatemi, E.: Nonlinear total variation based noise removal algorithms. *Physica D* **60**, 259–268 (1992)
44. Sarkar, N., Chaudhuri, B.B.: An efficient approach to estimate fractal dimension of textural images. *Pattern Recognit.* **25**(9), 1035–1041 (1992)
45. Shen, J.: Inpainting and the fundamental problem of image processing. *SIAM News* 36 (2003)
46. Starck, J., Elad, M., Donoho, D.: Image decomposition via the combination of sparse representations and a variational approach. *IEEE Trans. Image Process.* **14**, 1570–1582 (2005)

47. Tadmor, E., Athavale, P.: Multiscale image representation using integro-differential equations. *Inverse Probl. Imaging* **3**(4), 693–710 (2009)
48. Tadmor, E., Nezzar, S., Vese, L.: A multiscale image representation using hierarchical  $(BV; L^2)$  decompositions. *Multiscale Model. Simul.* **2**(4), 554–579 (2003)
49. Tadmor, E., Nezzar, S., Vese, L.: Multiscale hierarchical decomposition of images with applications to deblurring, denoising and segmentation. *Commun. Math. Sci.* **6**(2), 281–307 (2008)
50. Tuceryan, M., Jain, A.K.: Texture analysis. In: *Handbook of Pattern Recognition and Computer Vision*, pp. 235–276 (1993)
51. Vese, L., Osher, S.: Modeling textures with total variation minimization and oscillating patterns in image processing. *J. Sci. Comput.* **19**, 553–572 (2003)
52. Vese, L., Osher, S.: Image denoising and decomposition with total variation minimization and oscillatory functions. *J. Math. Imaging Vis.* **20**, 7–18 (2004)
53. Weiss, P., Aubert, G., Blanc-Féraud, L.: Efficient schemes for total variation minimization under constraints in image processing. *SIAM J. Sci. Comput.* **31**(3), 2047–2080 (2009)



**Liming Tang** received his M.S. degree in application mathematics from Chongqing University in 2007. He is currently working towards the Ph.D. degree in College of Mathematics and Statistics in Chongqing University. His research interests include the variation theory, partial differential equation and its applications in image processing.



**Chuanjiang He** is a professor and doctor tutor of Mathematics at College of Mathematics and Statistics in Chongqing University. He obtained the B.S. (1986) and M.S. (1989) in mathematics from Sichuan University, and Ph.D. (2004) from Chongqing University. His research interests include numerical calculation, partial differential equation and its applications.